

Why Water Reorientation Slows without Iceberg Formation around Hydrophobic Solutes

Damien Laage,^{*,†,‡} Guillaume Stirnemann,^{†,‡} and James T. Hynes^{†,‡,§}

Chemistry Department, Ecole Normale Supérieure, rue Lhomond, 75005 Paris, France, CNRS UMR 8640, rue Lhomond, 75005 Paris, France, and Department of Chemistry and Biochemistry, University of Colorado, Boulder, Colorado 80309-0215

Received: October 28, 2008

The dynamics of water molecules next to hydrophobic solutes is investigated, specifically addressing the recent controversy raised by the first time-resolved observations, which concluded that some water molecules are immobilized by hydrophobic groups, in strong contrast to previous NMR conclusions. Through molecular dynamics simulations and an analytic jump reorientation model, we identify the water reorientation mechanism next to a hydrophobic solute and provide evidence that no water molecules are immobilized by hydrophobic solutes. Their moderate rotational slowdown compared to bulk water (e.g., by a factor of less than 2 at low solute concentration) is mainly due to slower hydrogen-bond exchange. The slowdown is quantitatively described by a solute excluded volume effect at the transition state for the key hydrogen-bond exchange in the reorientation mechanism. We show that this picture is consistent with both ultrafast anisotropy and NMR experimental results and that the transition state excluded volume theory yields quantitative predictions of the rotational slowdown for diverse hydrophobic solutes of varying size over a wide concentration range. We also explain why hydrophobic groups slow water reorientation less than do some hydrophilic groups.

I. Introduction

Fundamental biochemical processes such as protein folding are driven by ubiquitous hydrophobic interactions, which are mediated by water.¹ However, whereas structural and thermodynamic aspects of hydrophobic hydration are now reasonably well understood,^{1–10} a comparable understanding of water dynamics next to a hydrophobic solute remains elusive. Very recently, a report of the first time-resolved measurements of proximal water reorientation in aqueous solutions of amphiphiles¹¹ concluded that two to four water molecules are immobilized by each methyl group, thus supporting the controversial iceberg picture¹² from a dynamical perspective, but conflicting with previous NMR interpretations^{13–17} and simulation results.^{18,19} The iceberg model explained the observed entropy decrease upon hydration of hydrophobic solutes by the structuring of water molecules into icelike cages around hydrophobic groups. Although its simplicity is appealing, this model has been seriously challenged,^{1,3} and despite an active search, the icelike structures have never been evidenced experimentally.²⁰

The time-resolved measurements¹¹ thus suggested that, although the cages' structure might be liquidlike, their dynamics is icelike. This interpretation relies on the observation of a large residual water anisotropy after delays that are long with respect to the 2.5-ps bulk water reorientation time. In particular, the results reproduced in Figure 1 were interpreted as reflecting the reorientation of two distinct types of water molecules: first, bulk waters that are unaffected by the hydrophobic solute's presence and, second, some water molecules within the hydration shell of the hydrophobic solute that are totally immobilized on the accessible experimental time scale (0–10 ps). In this model,

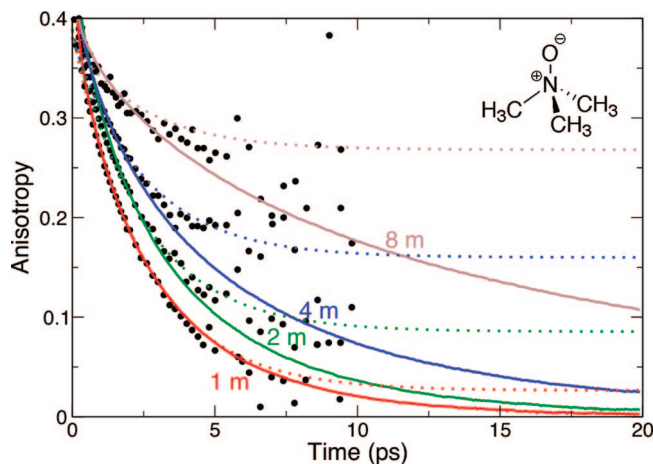


Figure 1. Anisotropy decay of water molecules' orientation in aqueous trimethylamine-*N*-oxide (TMAO) solutions of increasing concentration: experimental values (dots) from ref 11, our scaled simulation anisotropies,⁶⁰ and fits¹¹(dashes) of the experimental results assuming a bulk/immobilized picture.⁶¹

the immobilization is assumed to occur independently of the concentration: with increasing solute concentration, the inferred fraction of immobilized water molecules increases, whereas the relaxation times of the bulk and immobilized states remain unchanged.

However, the existence of this anisotropy plateau at long delays (and thus the validity of the model) can be questioned for several reasons. First, even if some water molecules were "frozen" onto a solute surface, the solute tumbling would be visible in the measured laboratory-frame anisotropy over the 0–10-ps interval.²¹ Second, this plateau appears at long delays, where the experimental values suffer from large uncertainties because of the small population remaining at these delays in

* Corresponding author. E-mail: damien.laage@ens.fr. Tel.: +33 1 44 32 24 18. Fax: +33 1 44 32 33 25.

[†] Ecole Normale Supérieure.

[‡] CNRS UMR 8640.

[§] University of Colorado.

the short-lived (lifetime of ~ 2 ps¹¹) vibrationally excited state and the necessarily approximate heating contribution correction.¹¹

In this article, we show through molecular dynamics simulations of various hydrophobic solutes in aqueous solutions that no water molecules are immobilized. We instead find a moderate (concentration-dependent) reorientational slowdown, that can be quantitatively described through an excluded volume effect at the transition state in the reorientation mechanism. These conclusions are shown to be consistent with the available experimental results, from both NMR and ultrafast infrared spectroscopies.

The outline of the remainder of this article is as follows: In section II, we detail our molecular dynamics simulation methodology. In section III, we detail the analysis of the water reorientation mechanism and the rate constant for water OH bonds initially next to the hydrophobic groups. In section IV, we show that the reorientational slowdown can be explained through transition state excluded volume arguments, and we demonstrate that this model provides quantitative estimates of the slowdown for various solute sizes over a wide concentration range. We end in section V with some concluding remarks.

II. Potentials and Methodology

We have performed classical molecular dynamics simulations of aqueous solutions of different hydrophobic solutes at different concentrations. All simulations employed the water SPC-E²² model, and different solute force fields [CH₄,²³ Xe,²⁴ tetramethylurea (TMU),²⁵ trimethylamine-*N*-oxide (TMAO),^{26,27} *tert*-butyl alcohol (TBA)^{26,28}]. The simulation boxes all contained a total of 500 particles, at the experimental density for TMU,²⁹ TMAO,^{27,30} and TBA^{31,32} (for CH₄ and Xe, no experimental density is available, and the low-concentration densities were estimated through *NPT* equilibration). The same procedure was followed at different concentrations, with only a change of the solution density and, therefore, of the simulation box size. The system was first equilibrated in the canonical ensemble at $T = 298$ K for 100 ps. The trajectory was then propagated in the microcanonical ensemble for more than 1 ns, with a 1-fs time step and periodic boundary conditions, treating the long-range electrostatic interactions through Ewald summation. The resulting average temperature was 298 ± 1 K.

The force field sensitivity of the calculated water reorientation times around the TMAO methyl groups was investigated by comparing rigid²⁶ and flexible²⁷ TMAO force fields. The rigid model²⁶ provided a better description of the available experimental translational diffusion constant^{26,33} and was therefore selected for the present work.

III. Water Reorientation Mechanism and Kinetics around Hydrophobic Groups

We have performed molecular dynamics simulations on concentrated trimethylamine-*N*-oxide (TMAO) aqueous solutions, for which the anisotropy decay had been measured experimentally.¹¹ The anisotropy, $R(t)$ is related to the second-order Legendre polynomial time-correlation function as $R(t) = \frac{2}{5} \langle P_2[\mathbf{u}(0) \cdot \mathbf{u}(t)] \rangle$, where \mathbf{u} designates the orientation of the water OH bond. The calculated anisotropy shown in Figure 1 reproduces well the experimental data at all concentrations for short (<5-ps) delays; for longer times, the simulated values are consistent with the experimental ones, which bear a large uncertainty. The calculated anisotropy decay shows a steady decrease at all delays and confirms the absence of a plateau. (However, we note that fits of the simulated anisotropies

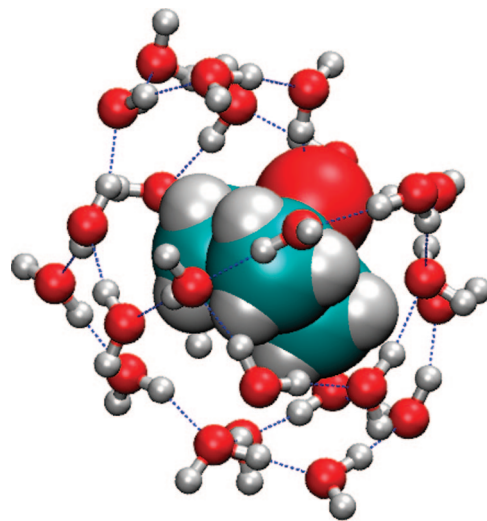


Figure 2. Typical hydration structure of TMAO, with a clathrate-like arrangement around the hydrophobic moiety.

restricted to the experimental 0–10-ps range would lead to nonvanishing plateau values.) The contrast with the immobilized/bulk model picture is even sharper for very long delays, inaccessible experimentally, where the anisotropy decays below values corresponding to one immobilized water molecule per solute molecule. There is no sign of any immobilized water at all, at any concentration. Instead, there is evidence for a quite different feature: a reorientational slowdown due to increasing solute concentration.

To focus on the effect from a single hydrophobic solute on the water behavior, we first simulated a dilute 0.1 *m* TMAO aqueous solution. If the bulk/immobilized model were valid, several water molecules (12 water OH groups¹¹) should be immobilized even at this low concentration. Our simulations showed that the three TMAO methyl substituents are hydrated together as a single large hydrophobic group, with the typical clathrate-like arrangement⁵ in which each water molecule has at least one OH bond tangent to the hydrophobic surface (Figure 2).

Whereas the structure of the water hydrogen-bond network is little affected by hydrophobic solutes,²⁰ the water rotational dynamics is a much more sensitive probe of lability. Two of us recently suggested^{34–36} that, beyond an initial <200-fs period in which a water OH group librates around its hydrogen-bond axis, the OH reorientation proceeds along two independent pathways. The first and most important route is via the exchange of H-bond acceptors, where, once the environment has reorganized to offer a new viable H-bond acceptor, the water OH bond suddenly executes a large-amplitude angular jump from its former H-bond partner to this new acceptor.³⁴ A second, additional minor contribution to the reorientation is through the slower diffusive reorientation of the intact H-bond axis (frame) between successive jumps.³⁴ The analytic extended jump model (EJM) associated with this mechanism successfully describes the reorientational dynamics of water in the bulk³⁴ and around a halide ion,³⁵ reproducing both the experimental and simulated reorientation times.^{34–36} Subsequent experiments supported the EJM.³⁷

Within this framework, we analyze the reorientation of a water OH group initially tangent to the TMAO hydrophobic moiety and contrast it with the bulk situation. We find a jump mechanism in the vicinity of TMAO, which is depicted in Figure 3a. Figure 3b shows the simulation data supporting this

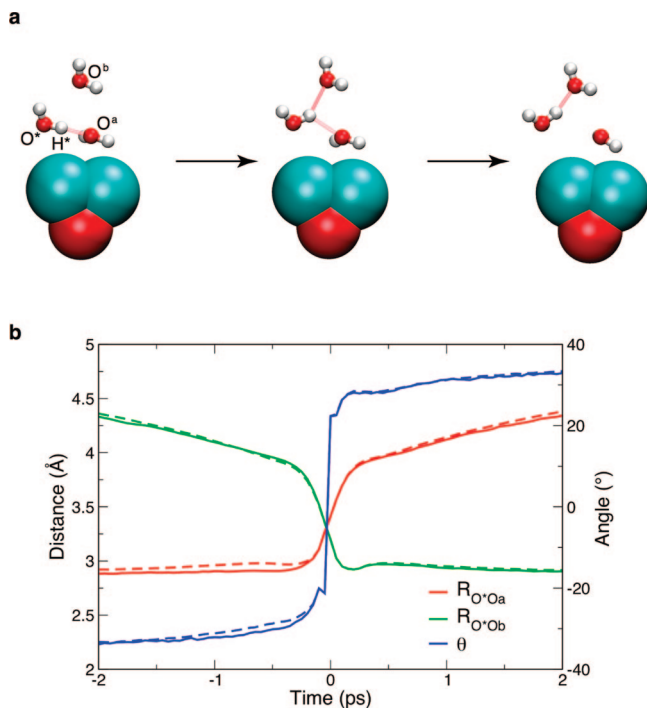


Figure 3. Jump reorientation and H-bond exchange mechanism next to a hydrophobic site. (a) Schematic representation of the successive steps in the mechanism for a water molecule initially in the hydration shell of TMAO's hydrophobic methyl groups. (b) Average time evolution of key distances and angle during the H-bond exchange and jump reorientation,³⁴ for a water molecule initially in the hydration shell of TMAO's methyl groups (solid lines) or in the bulk situation (dashes).

mechanism, with the average time evolution of some key distances and the angle during the H-bond exchange: $R_{O^*O^a}$ and $R_{O^*O^b}$ are the distances between the central water oxygen and the initial (O^a) and final (O^b) acceptors, θ is the angle between the O^*-H^* bond and the bisector plane of the $O^aO^*O^b$ angle, defined such that $\theta = 0^\circ$ when H^* lies on the bisector plane and $\theta < 0^\circ$ when H^* lies on the O^a side; the time origin $t = 0$ is chosen when $\theta = 0^\circ$. The reorienting water OH group is initially H-bonded to another water within the hydrophobic hydration shell. This H-bond then elongates as a new water partner arrives from the second shell. At the transition state for this "reaction", the rotating water molecule forms a symmetric bifurcated H-bond with its two equivalent initial and final water acceptors. The reorienting water molecule then leaves the hydrophobic first shell, and the new H-bond stabilizes. As evidenced for neat water,³⁶ individual reorientation trajectories are distributed around this average path. This mechanism is identical to that determined in neat water, as evidenced by the comparison of the average mechanisms (Figure 3b) and the same average jump amplitude $\Delta\theta$ (Table 1). However, the associated jump time, τ_{jump} , computed as the inverse rate constant for the replacement of a stable $O-H\cdots O$ bond by another stable $O-H\cdots O$ bond,³⁴⁻³⁶ is somewhat slower around TMAO's hydrophobic groups than in the bulk, as now discussed.

Within the EJM, the overall reorientation time, τ_{reor} , is calculated³⁴ from the jump reorientation together with the slower τ_{frame} reorientation of an intact H-bond, determined from the orientational relaxation between the jump events, as

$$\frac{1}{\tau_{\text{reor}}} = \frac{1}{\tau_{\text{jump}}} \left[1 - \frac{1 \sin(5\Delta\theta/2)}{5 \sin(\Delta\theta/2)} \right] + \frac{1}{\tau_{\text{frame}}} \quad (1)$$

Table 1 shows that this reorientation time, τ_{reor} , which agrees well with the direct simulation results, is retarded by a factor of only 1.5 in the vicinity of the hydrophobic groups, the effect coming mainly from the slower jump time (the frame contribution remains minor, despite its marked slowing around the methyl groups). This moderate slowdown sharply contrasts with the immobilization over the 0–10-ps period assumed by the bulk/immobilized two-state model¹¹ even at low concentration.

An alternate determination of the water reorientational slowdown next to three methyl groups is provided by NMR spectroscopy. When the majority of the work of the present article was completed, the only available measurements were on aqueous solutions of *tert*-butyl alcohol [TBA, $(\text{CH}_3)_3\text{COH}$]^{13,17}, which is structurally very close to TMAO, with an identical hydrophobic moiety but a different hydrophilic head; results for TMAO became available subsequently.³⁸ For both solutes, we determine the water reorientational slowdown factor around the hydrophobic methyl groups from dilute 0.1 *m* simulations; the two values are very similar: approximately 1.4 for TBA vs 1.5 for TMAO (Table 1). The NMR spin relaxation rate, R_1 , is proportional to the water reorientation time, but because NMR spectroscopy is not time-resolved, this reorientation time is averaged over all different environments in the solution, i.e., the bulk and solute hydration layer. The influence of the solute is isolated for dilute solutions, where the spin relaxation rate depends linearly on the solute molality m ^{13,17,38,39}

$$\frac{R_1}{R_1^{\text{blk}}} = \frac{\langle \tau_{\text{reor}} \rangle}{\tau_{\text{reor}}^{\text{blk}}} = 1 + Bm \quad (2)$$

where R_1 , R_1^{blk} and $\langle \tau_{\text{reor}} \rangle$, $\tau_{\text{reor}}^{\text{blk}}$ are the spin relaxation rates and the average water reorientation times, respectively, for the entire solution at molality m and for bulk water and B is a proportionality factor. NMR studies^{13,17,38,39} then infer from B an average water reorientation retardation factor around the solute. However, this factor should be considered with care, as it depends on the value used for the solute hydration number and is averaged over situations with very different reorientation times. This is evidenced by our simulations on TBA and TMAO, which show that, whereas water OH bonds initially tangent to the hydrophobic groups have a retardation factor of respectively 1.4 and 1.5, the OH bonds pointing out of the hydrophobic shell are nearly bulk-like (~ 1.2 and ~ 1.3), whereas the OH bonds pointing toward the hydrophilic site exhibit retardation factors which strongly depend on the strength of the H-bond acceptor (~ 1.2 for the hydroxyl group of TBA vs ~ 2.4 for the negatively charged oxygen of TMAO).⁴⁰ The number of OH bonds in these additional groups is relatively small, and the resulting average retardation factor is close to the value around the hydrophobic side. However, we prefer to directly calculate the average reorientation time concentration dependence for a series of simulated dilute solutions to compare the simulated B values with the experimental ones: the agreement is excellent for TMAO and fair for TBA, where our simulations somewhat underestimate the reorientational slowdown (see Figure 4). Our simulations therefore reproduce the NMR raw results and agree with the NMR interpretation,^{13,17,38,39} confirming the limited retardation induced by methyl groups on the water reorientational dynamics.

Because NMR spectroscopy measures a reorientational slowdown averaged over the entire solute hydration layer,^{13,39} it might be argued¹¹ that the moderate average slowdown observed by NMR spectroscopy for TBA,^{13,17} TMAO,³⁸ and

TABLE 1: Reorientation Times for a Water OH Bond Initially Next to a Hydrophobic Group of TMAO or in the Bulk

environment	jump time, τ_{jump} (ps)	jump amplitude, $\Delta\theta$ (deg)	frame reorientation time, ^a τ_{frame} (ps)	extended jump model reorientation time, ^b τ_{reor} (ps)	reorientation retardation factor, $\tau_{\text{reor}}/\tau_{\text{reor}}^{\text{bulk}}$
hydrophobic ^c	4.5 (4.5)	68 (68)	10.8 (7.4)	3.4 (2.8)	1.5 (1.3)
bulk	3.3	68	5.9	2.2	1

^a Reorientation times associated with the second-order Legendre polynomial orientational time-correlation. ^b The orientational time correlation function calculated from the simulations for a water molecule initially in the hydrophobic hydration layer does not rigorously provide the reorientation time because it contains a bulk contribution at long delays.³⁵ However, these approximate reorientation times (2.5 and 4.0 ps for bulk water and around the rigid hydrophobic group, respectively) agree well with the extended jump model predictions and lead to the same retardation factor. If the model is refined to consider the $\Delta\theta$ jump angle distribution,³⁶ this agreement is excellent (2.5 and 3.8 ps from the improved model for bulk water and around the rigid hydrophobic group, respectively). ^c Values indicated for the TMAO rigid force field²⁶ and within parentheses for the flexible force field²⁷ for comparison (the rigid force field is more appropriate for the dynamics).

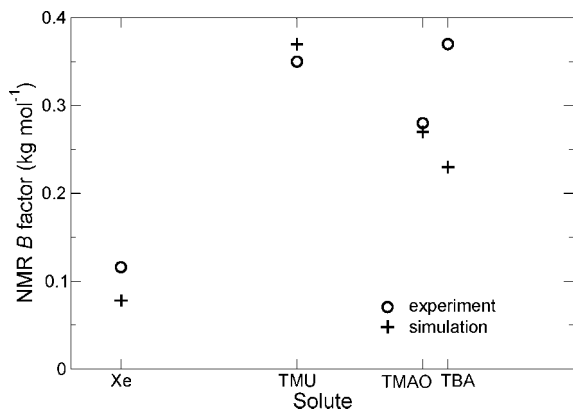


Figure 4. Comparison of our simulation B factors with the experimental NMR results for xenon,¹⁴ tetramethylurea,¹⁵ trimethylamino- N -oxide³⁸ and *tert*-butyl alcohol.¹³

various other solutes containing hydrophobic groups^{16,17} results from the averaging of two subsets of waters, some immobilized and others bulk-like. From our simulations, the total number of water molecules within the TMAO and TBA hydration layers in 0.1 m dilute solutions is 19 and 21, respectively (in agreement with recent neutron scattering experiments⁴¹), leading to 24 and 27 water OH groups tangent to the methyl groups. According to ref 11, 12 OH groups are immobilized by TBA or TMAO, thus representing a subset of all the tangent OH bonds. Such heterogeneity seems incompatible with the symmetry of the hydrophobic moiety and is absent from our simulations.

IV. Quantitative Description of the Reorientational Slowdown

a. Slowdown around a Single Solute. Figure 3b shows that the TMAO hydrophobic group does not retard the H-bond exchange reaction dynamics by constraining the system to pass through a different, higher-energy, transition state, given that, as noted in section III, the average jump mechanisms are identical in the bulk and next to TMAO's hydrophobic sites. Instead, the approach of a new water partner—a key feature of that mechanism^{34,36}—is hindered by the excluded volume induced by the neighboring hydrophobic group. The number of accessible transition state configurations is therefore reduced. A simple transition-state-theory⁴²-type argument for the H-bond exchange reaction shows that the jump time in eq 1, which Table 1 indicates is largely responsible for the slowdown, is inversely proportional to the accessible transition state volume Ω^\ddagger

$$\tau_{\text{jump}} \propto \exp\left(\frac{\Delta G^\ddagger}{k_B T}\right) = \exp\left(\frac{-\Delta S^\ddagger}{k_B} + \frac{\Delta H^\ddagger}{k_B T}\right) \approx \frac{\Omega^R}{\Omega^\ddagger} \exp\left(\frac{\Delta H^\ddagger}{k_B T}\right) \propto \frac{1}{\Omega^\ddagger} \quad (3)$$

where the activation entropy contribution, ΔS^\ddagger , to the activation free energy, ΔG^\ddagger , has been approximated as $k_B \ln(\Omega^R/\Omega^\ddagger)$. In the bulk (Figure 3b), the transition state locations for the new water partner lie along a ring defined by a distance to the reorienting water of $R^\ddagger \approx 3.5$ Å and an attack angle with respect to the initial H-bond axis of $\Delta\theta = 68^\circ$. The fraction, f , of this ring which falls within the hydrophobic solute excluded volume provides the complementary fraction, $1 - f$, of accessible transition states (Figure 5). Assuming that the reactant volume, Ω^R , is unchanged⁴³ and that the change in the activation enthalpy, ΔH^\ddagger , can be neglected, as suggested by the very minor H-bond energy increase around hydrophobic groups,¹⁸ this leads to the slowdown factor

$$\frac{\tau_{\text{jump}}^{\text{hydrophobic}}}{\tau_{\text{jump}}^{\text{bulk}}} = \frac{1}{1 - f} \quad (4)$$

Previous work has recognized that hydrophobic groups induce a steric effect causing a slowdown of H-bond rearrangements.^{18,44,45} In the present work, the knowledge of the transition state configuration for H-bond exchange required in the reorientation mechanism leads directly to a quantitative expression for the reorientational slowdown factor by measuring the appropriate excluded volume. The activation entropy that retards the proximal water dynamics is to be contrasted with the entropic contribution to the hydrophobic hydration free energy for small solutes,^{2,3,6,7} although they both stem from the existence of a hydrophobic cavity.

The transition state excluded volume (TSEV) fraction, f , can be determined either geometrically if the hydrophobic group is approximately spherical or from the molecular dynamics simulations. In the simple spherical case, f is the fraction of the ring of possible transition state locations for the new oxygen acceptor O^b (defined by $O^*O^b = R^\ddagger$ and $O^aO^*O^b = \Delta\theta$; see Figure 3) that overlaps the hydrophobic exclusion sphere of radius R centered on the hydrophobic group. The geometric derivation detailed in the Appendix leads to the analytic retardation factor

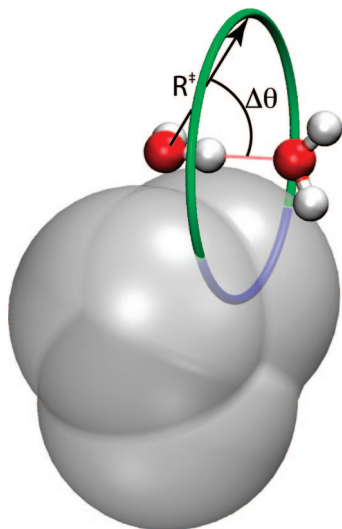


Figure 5. Transition state geometries for the H-bond exchange excluded by the presence of a hydrophobic group. Possible transition state locations for the new H-bond acceptor O^b lie on the ring defined by $R_{O^b} = R^\ddagger$ and $O^b\hat{O}^*O^b = \Delta\theta$. The fraction of this ring that overlaps with the excluded volume of the TMAO methyl groups is represented in blue, and the accessible fraction is shown in green.

$$\frac{\tau_{\text{jump}}^{\text{hydrophobic}}}{\tau_{\text{jump}}^{\text{bulk}}} = \frac{1}{1-f} = \left\{ 1 - \frac{1}{\pi} \cos^{-1} \left[\frac{(R^\ddagger)^2 + 2rR + r^2 - dR^\ddagger \cos(\Delta\theta)}{2R^\ddagger \sin(\Delta\theta) \sqrt{(R+r)^2 - (d/2)^2}} \right] \right\}^{-1} \quad (5)$$

where r is the distance between the hydration layer and the surface of the excluded sphere and d is the average oxygen–oxygen distance within the hydration layer. The effective radius R used in this analytic calculation is determined as the largest distance from the center of the sphere for which the water oxygen radial distribution function is zero. For solutes that are not strictly spherical, the sphere is centered on the hydrophobic group, e.g., $\text{N}(\text{CH}_3)_3$ for TMAO, $\text{C}(\text{CH}_3)_3$ for TBA, and $\text{N}(\text{CH}_3)_2$ for each of the two dimethylamino groups of TMU. The remaining parameters were found to be nearly solute-independent.

The TSEV fraction can also be calculated numerically from the molecular dynamics simulations. Along the trajectory, for each water molecule lying within the hydrophobic hydration layer, its H-bond acceptor is identified, and the transition state ring defined by R^\ddagger and $\Delta\theta$ (see Figure 5) is sampled in 200 evenly spaced points. f is calculated as the fraction of these points falling within the solute excluded volume, defined as the superposition of spheres centered on each solute atom, whose respective radii are the largest distance for which the radial distribution function between this solute atom and the water oxygen atoms is zero.

As shown in Table 2 for a range of solutes in dilute solutions, the analytic TSEV fraction in eq 4 is in good agreement with the simulation calculation. Although the analytic model provides the explicit TSEV dependence on each parameter, the simulation approach is better suited for very nonspherical solutes or for high-concentration solutions where multiple hydrophobic sites can surround a single water molecule, which cannot be described by the analytic expression in eq 4.

Next to a convex solute of increasing radius (at low concentration), the TSEV fraction f increases from 0 to $1/2$ next to a hydrophobic plane where one-half of the space is excluded,⁴⁶ and the slowdown factor $1/(1-f)$ accordingly increases from

TABLE 2: Comparison of Analytic and Simulation Determinations of the Excluded Volume Fraction f

solute	effective radius R	excluded volume fraction f	
		analytic (eq 4)	simulation
CH ₄	2.8	0.28	0.28
Xe	3.2	0.30	0.29
TMU	3.9	0.32	0.30
TMAO	4.4	0.33	0.33
TBA	4.5	0.33	0.32

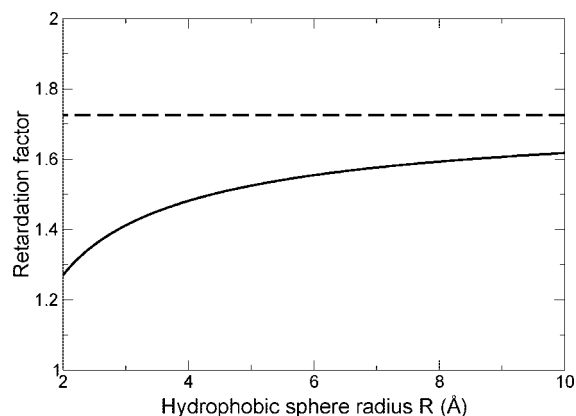


Figure 6. Retardation factor calculated analytically from eq 4 as a function of the hydrophobic sphere radius R for the typical values $R^\ddagger = 3.5$ Å, $\Delta\theta = 68^\circ$, $r = 0.8$ Å, and $d = 2.8$ Å, which were found to be nearly solute-independent. The dashes indicate the asymptotic value for infinite R (See Appendix).

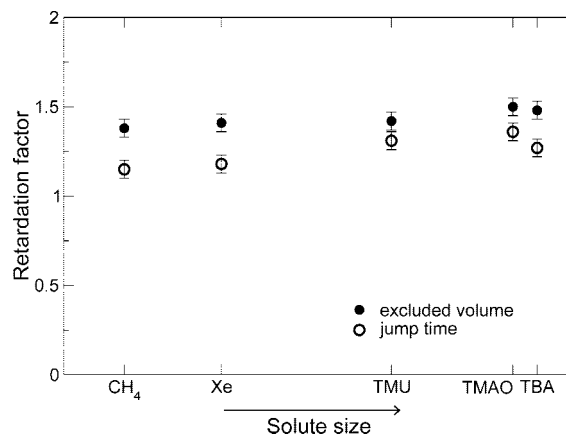


Figure 7. Retardation factor as a function of solute size for a water OH bond initially tangent to the solute. The retardation factor is determined both by TSEV eq 3 evaluated numerically and by the ratio of jump times from the simulations, as a function of the hydrophobic solute size, for methane, xenon, tetramethylurea (two separate pairs of methyl groups), trimethylamino-*N*-oxide, and *tert*-butyl alcohol.

1 to a maximum value of 2 (Figure 6).⁴⁷ The slowdown predicted by the TSEV calculation can be compared in Figure 7 with simulated H-bond exchange retardations for hydrophobic solutes of increasing size, ranging from methane to TBA; the predictions are semiquantitative and confirm that the slowdown factor varies very little with solute size and remains below 2. This explains why the slowdowns measured by NMR spectroscopy^{16,17} (or dielectric relaxation⁴⁸) on a wide range of hydrophobic solutes with diverse sizes and functional groups are all similar and very moderate, with values below 2.

Because the hydrophobic solute acts only through its TSEV, this explains why the components of the jump reorientation time and the retardation factors (dominated by these components) are only slightly affected by the solute force field, as shown by

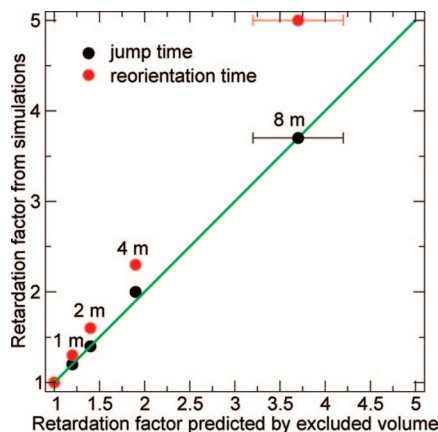


Figure 8. Retardation factor as a function of TMAO concentration for a water OH bond initially tangent to the solute. Comparison of the retardation factors predicted by numerical evaluation of TSEV eq 3 and determined as the ratio of hydrophobic vs bulk jump times and reorientation times, for increasing TMAO molality.⁶² Except at 8 m, the error bars lie within the dot size.

the comparison between rigid and flexible force fields in Table 1. The reorientational jumps involve only water acceptors, whose force field is unchanged.

b. Extension to Concentrated Solutions. TSEV considerations also explain and reproduce the overall water reorientation slowdown for increasing solute concentration, as observed, for example, in the simulation results for TMAO in Figure 1. For concentrated solutions, water molecules are surrounded by more than one hydrophobic group, the TSEV fraction f increases beyond $1/2$, and the retardation factor $1/(1-f)$ exceeds 2. The decreasing accessible transition state volume quantitatively describes the H-bond exchange retardation with increasing concentration in the entire 0–8 m range for TMAO (Figure 8). The slowdown becomes more pronounced for reorientation than for H-bond exchange because of the additional slowdown of the frame reorientation component (eq 1) due to the increasing solution viscosity. Accordingly, the water reorientation time lengthens for increasing concentrations, in contrast to the assumption of the bulk/immobilized model.

The TSEV model also provides an interpretation of the anisotropy decay averaged over all water OH bonds within the solution, as calculated or measured by ultrafast spectroscopy (e.g., Figure 1). We calculated the probability distribution of the jump time TSEV slowdown factors $\rho = 1/(1-f)$ for all of the water OH bonds (except for the few pointing toward the solute hydrophilic site) within TMAO solutions of increasing concentration (Figure 8). In the low-molality 1 m case, the bulk water molecules induce a narrow peak with no slowdown ($\rho = 1$), whereas the water OH bonds in the vicinity of the solute molecules lead to a broader distribution for moderate slowdown values. With increasing concentration, the bulk peak recedes, and the distribution of slowdown factors broadens and extends to higher values. At 8 m, no bulk is left. Several interpretations of the high-concentration anisotropy decay have already been suggested: within the bulk/immobilized model,¹¹ this decay results from the two separate immobilized and bulk populations and is modeled by the sum of an exponential plus a constant term; more recently,³⁸ it was suggested the decay is biexponential, reflecting two distinct reorientation time scales within the hydration shell. In contrast to these suggestions, Figure 9 shows that, at high concentration, the anisotropy decay does not originate from two separate populations and is not biexponential. The decay instead comes from a broad distribution of

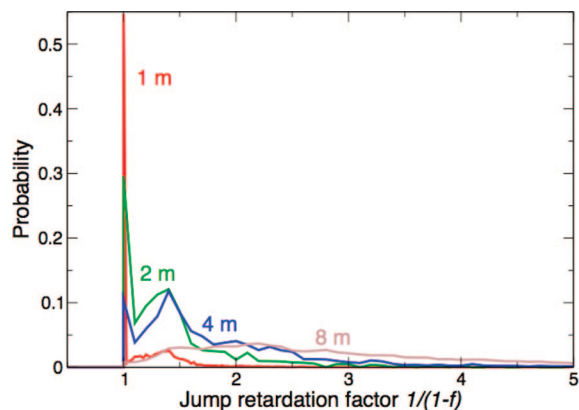


Figure 9. Probability distributions of the TSEV retardation factor for the TMAO aqueous solutions of increasing concentration whose anisotropy decay is shown in Figure 1.

slowdown factors depending on the local environment, which explains the stretched-exponential character of the anisotropy decay, as observed for water around proteins.¹

Despite the successes of the TSEV model recounted above, the model has limitations. The model explains the reorientation slowdown through considerations that are purely entropic⁴⁹ and, therefore, does not predict any temperature dependence of the retardation factor. However, experimentally, a very weak decrease of the slowdown factor that appears to be solute-dependent has been observed for increasing temperature within the liquid range.^{13,14,17,38} A first explanation lies in the model's neglect of the small activation enthalpy difference next to the hydrophobic groups and in the bulk. A second explanation lies in the different temperature dependences of the transmission coefficients correcting the transition state theory rate constant³⁶ next to the hydrophobic groups and in the bulk; the transmission coefficient temperature dependence was shown to be an important contribution to the overall temperature dependence of the reorientation time in bulk water.³⁶ Both of these aspects are currently under investigation.

V. Concluding Remarks

We have performed molecular dynamics simulations of aqueous solutions of various hydrophobic solutes, for a wide range of concentrations. We found that, in dilute solutions, the rate of water reorientation in the vicinity of the hydrophobic solutes is decreased only moderately, in contrast to the behavior predicted by the proposed bulk/immobilized model.¹¹ The simulations show that this slowdown becomes more important for increasing solute concentration. The reorientation mechanism and rate constants are well described by the extended jump model.

Simple transition state excluded volume considerations within the framework of the extended jump model were shown to predict the slowdown of water H-bond dynamics around a hydrophobic site and to explain why the solute size has little influence on the slowdown. At low concentration, the factor always remains below 2, in accord with NMR experiments.^{13–17,38} No hydrophobic dynamic icebergs are formed. This model also explains why larger (>2) slowdown factors are observed experimentally only for either high solute concentrations¹¹ or hydrophilic solutes^{50,51} for which the reorienting water is initially H-bonded to the solute: the H-bond exchange mechanism and therefore the activation enthalpy barrier are modified.³⁶ Hydrophobic groups are therefore weak water reorientation retardants with respect to some hydrophilic groups.

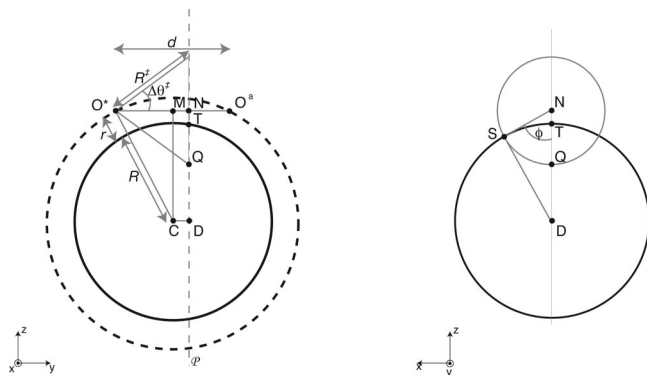


Figure 10. Schematic representations of cuts through the hydrophobic sphere and its hydration layer.

Ideas closely related to those of this work should prove useful in understanding water dynamics in complex environments, such as proteins,⁵² DNA,^{53,54} and confined media such as nanopores^{55,56} or reverse micelles.^{57–59}

Acknowledgment. Peter Rossky (University of Texas, Austin, TX) is gratefully acknowledged for his comments on the manuscript. This work was supported in part by NSF Grants CHE-0417570 and CHE-0750477.

Appendix: Geometrical Derivation of the Excluded Volume Fraction

For a spherical hydrophobic group (see Figure 10), the key parameters to determine the TSEV are R , the radius of the hydrophobic excluded sphere; r , the distance between the hydration layer (peak of the hydrophobic group–water oxygen radial distribution function, $g_{\text{O}}(r)$) and the hydrophobic excluded sphere (where $g_{\text{O}}(r)$ is no longer zero); R^{\ddagger} and $\Delta\theta$, which define the transition state ring; and d , the average distance between two water oxygens within the hydration layer, determined from the oxygen–oxygen radial distribution function. The fraction of excluded transition state volume is the fraction of the transition state circle centered on N that overlaps the hydrophobic exclusion circle centered in D and thus $f = \phi/\pi$. The angle ϕ is defined in the NSD triangle by

$$\phi = \cos^{-1}\left(\frac{\overline{SN}^2 + \overline{ND}^2 - \overline{SD}^2}{2\overline{SN}\overline{ND}}\right)$$

Each side of the triangle can be determined as follows

$$\begin{aligned}\overline{SN} &= \overline{NQ} = R^{\ddagger} \sin(\Delta\theta) \\ \overline{SD} &= \overline{TD} = \sqrt{\overline{CT}^2 - \overline{CD}^2} = \sqrt{R^2 - \overline{MN}^2} = \\ &= \sqrt{R^2 - [R^{\ddagger} \cos(\Delta\theta) - d/2]^2} \\ \overline{ND} &= \overline{MC} = \sqrt{\overline{O^*C}^2 - \overline{O^*M}^2} = \sqrt{(R+r)^2 - (d/2)^2}\end{aligned}$$

Hence

$$f = \frac{1}{\pi} \cos^{-1}\left[\frac{2Rr + r^2 + (R^{\ddagger})^2 - R^{\ddagger}d \cos(\Delta\theta)}{2R^{\ddagger} \sin(\Delta\theta) \sqrt{(R+r)^2 - (d/2)^2}}\right]$$

This expression is valid when the transition state ring intercepts the hydrophobic sphere, i.e., for $R > d/2 - r$, $R > |R^{\ddagger} \cos(\Delta\theta) - d/2|$, and when the inverse cosine argument is <1 . For an increasing solute radius R , the excluded volume fraction asymptotically converges to

$$f \xrightarrow{R \rightarrow \infty} \frac{1}{\pi} \cos^{-1}\left[\frac{r}{R^{\ddagger} \sin(\Delta\theta)}\right]$$

which is $1/2$ for $r = 0$.

References and Notes

- (1) Ball, P. *Chem. Rev.* **2008**, *108*, 74–108.
- (2) Chandler, D. *Nature* **2005**, *437*, 640–647.
- (3) Blokzijl, W.; Engberts, J. B. F. N. *Angew. Chem., Int. Ed.* **1993**, *32*, 1545–1579.
- (4) Lee, S. H.; Rossky, P. J. *J. Chem. Phys.* **1994**, *100*, 3334.
- (5) Cheng, Y. K.; Rossky, P. J. *Nature Phys.* **1998**, *392*, 696–699.
- (6) Hummer, G.; Garde, S.; Garcia, A. E.; Pohorille, A.; Pratt, L. R. *Proc. Natl. Acad. Sci. U.S.A.* **1996**, *93*, 8951.
- (7) Hummer, G.; Garde, S.; Garcia, A. E.; Paulaitis, M. E.; Pratt, L. R. *J. Phys. Chem. B* **1998**, *102*, 10469.
- (8) Southall, N. T.; Dill, K. A.; Haymet, A. D. J. *J. Phys. Chem. B* **2002**, *106*, 521.
- (9) Gallagher, K. R.; Sharp, K. A. *J. Am. Chem. Soc.* **2003**, *125*, 9853.
- (10) Raschke, T. M.; Levitt, M. *Proc. Natl. Acad. Sci. U.S.A.* **2005**, *102*, 6777–6782.
- (11) Rezus, Y. L. A.; Bakker, H. J. *Phys. Rev. Lett.* **2007**, *99*, 148301.
- (12) Frank, H. S.; Evans, M. W. *J. Chem. Phys.* **1945**, *13*, 507–532.
- (13) Yoshida, K.; Ibuki, K.; Ueno, M. *J. Chem. Phys.* **1998**, *108*, 1360–1367.
- (14) Haselmeier, R.; Holz, M.; Marbach, W.; Weingartner, H. *J. Phys. Chem.* **1995**, *99*, 2243.
- (15) Shimizu, A.; Fumino, K.; Yukiyasu, K.; Taniguchi, Y. *J. Mol. Liq.* **2000**, *85*, 269.
- (16) Okouchi, S.; Moto, T.; Ishihara, Y.; Numajiri, H.; Uedaira, H. *J. Chem. Soc., Faraday Trans.* **1996**, *92*, 1853.
- (17) Ishihara, Y.; Okouchi, S.; Uedaira, H. *J. Chem. Soc., Faraday Trans.* **1997**, *93*, 3337.
- (18) Rossky, P. J.; Karplus, M. *J. Am. Chem. Soc.* **1979**, *101*, 1913.
- (19) Zichi, D. A.; Rossky, P. J. *J. Chem. Phys.* **1986**, *84*, 2814.
- (20) Buchanan, P.; Aldiwan, N.; Soper, A. K.; Creek, J. L.; Koh, C. A. *Chem. Phys. Lett.* **2005**, *415*, 89.
- (21) Our simulations of dilute TMAO solutions yield a second-order reorientation time of the TMAO N–O axis of 14 ps, consistent with the first-order Debye relaxation time of 30 ps measured experimentally: Shikata, T.; Itatani, S. *J. Solution Chem.* **2002**, *31*, 823–844. The NO anisotropy thus decays by more than 50% on the 0–10-ps interval.
- (22) Berendsen, H. J. C.; Grigera, J. R.; Straatsma, T. P. *J. Phys. Chem.* **1987**, *91*, 6269.
- (23) Grossman, J. C.; Schwegler, E.; Galli, G. *J. Phys. Chem. B* **2004**, *108*, 15865.
- (24) Straatsma, T. P.; Berendsen, H. J. C.; Postma, J. P. M. *J. Chem. Phys.* **1986**, *85*, 6720.
- (25) Belletato, P.; Freitas, L. C. G.; Areas, E. P. G.; Santos, P. S. *Phys. Chem. Chem. Phys.* **1999**, *1*, 4769.
- (26) Paul, S.; Patey, G. N. *J. Phys. Chem. B* **2006**, *110*, 10514.
- (27) Kast, K. M.; Brickmann, J.; Kast, S. M.; Berry, R. S. *J. Phys. Chem. A* **2003**, *107*, 5342.
- (28) Fornili, A.; Civera, M.; Sironi, M.; Fornili, S. L. *Phys. Chem. Chem. Phys.* **2003**, *5*, 4905.
- (29) Patil, K. J.; Sargar, A. M.; Dagade, D. H. *Indian J. Chem. A: Inorg., Bio-inorg., Phys., Theor. Anal. Chem.* **2002**, *41*, 1804.
- (30) Zou, Q.; Bennion, B. J.; Daggett, V.; Murphy, K. P. *J. Am. Chem. Soc.* **2002**, *124*, 1192.
- (31) Broadwater, T. L.; Kay, R. L. *J. Phys. Chem.* **1970**, *74*, 3802.
- (32) Nakanishi, K.; Kato, N.; Maruyama, M. *J. Phys. Chem.* **1967**, *71*, 814.
- (33) In a 4 m aqueous TMAO solution, the experimental water translational diffusion constant is $0.54 \times 10^{-5} \text{ cm}^2 \text{ s}^{-1}$; the rigid model leads to a $1.0 \times 10^{-5} \text{ cm}^2 \text{ s}^{-1}$ value, in better agreement than the flexible model, which yields a diffusion constant of $1.5 \times 10^{-5} \text{ cm}^2 \text{ s}^{-1}$.
- (34) Laage, D.; Hynes, J. T. *Science* **2006**, *311*, 832–835.
- (35) Laage, D.; Hynes, J. T. *Proc. Natl. Acad. Sci. U.S.A.* **2007**, *104*, 11167–11172.
- (36) Laage, D.; Hynes, J. T. *J. Phys. Chem. B* **2008**, *112*, 14230.
- (37) (a) Loparo, J. J.; Roberts, S. T.; Tokmakoff, A. *J. Chem. Phys.* **2006**, *125*, 194522. (b) Bakker, H. J.; Rezus, Y. L. A.; Timmer, R. L. A. *J. Phys. Chem. A* **2008**, *112*, 11523–11534.
- (38) Qvist, J.; Halle, B. J. *Am. Chem. Soc.* **2008**, *130*, 10345.
- (39) Hertz, H. G.; Zeidler, M. D. *Ber. Bunsen-Ges. Phys. Chem.* **1964**, *68*, 821.
- (40) These retardation factors were determined from the anisotropy decay times for water OH bonds initially next to each of the solute sites. These decay times are approximations, as the residence time of water next to these sites is comparable to the anisotropy decay value.

- (41) Nakada, M.; Yamamuro, O.; Maruyama, K.; Misawa, M. *J. Phys. Soc. Jpn.* **2007**, *76*, 054601.
- (42) Glasstone, S.; Laidler, K. J.; Eyring, H. *The Theory of Rate Processes*; McGraw-Hill: New York, 1941.
- (43) The reactant state is defined by the existence of a H-bond with the initial partner, without any restriction on the new partner location. The presence of the hydrophobic group, therefore, does not impose any limitation on the accessible reactant states.
- (44) Sciortino, F.; Geiger, A.; Stanley, H. E. *Nature* **1991**, *354*, 218–221.
- (45) Xu, H. F.; Berne, B. J. *J. Phys. Chem. B* **2001**, *105*, 11929–11932.
- (46) However, next to an extended hydrophobic surface, the H-bond arrangement is no longer clathrate-like,^{2,5} and our model should be extended to include the OH bonds pointing toward the surface.
- (47) In ref 11, a steric factor associated with the attainment of the five-coordinate transition state (originally found in ref 34 and found again in the present work) was invoked to explain the immobilization. However, in dilute solutions, the transition-state excluded volume fraction cannot exceed $1/2$, and the maximum slowdown is 2, very far from immobilization.
- (48) Hallenga, K.; Grigera, J. R.; Berendsen, H. J. C. *J. Phys. Chem.* **1980**, *84*, 2381–2390.
- (49) The entropic factor was also assumed to be temperature-independent through its microcanonical expression in eq 3.
- (50) See within; for TMAO, the more pronounced slowdown is around the hydrophilic head (~ 2.4) rather than around the hydrophobic moiety (~ 1.5).
- (51) Belton, P. S.; Ring, S. G.; Botham, R. L.; Hills, B. P. *Mol. Phys.* **1991**, *72*, 1123.
- (52) Denisov, V. P.; Halle, B. *Faraday Discuss.* **1996**, 227.
- (53) Pal, S.; Maiti, P. K.; Bagchi, B.; Hynes, J. T. *J. Phys. Chem. B* **2006**, *110*, 26396.
- (54) Pal, S. K.; Zhao, L. A.; Zewail, A. H. *Proc. Natl. Acad. Sci. U.S.A.* **2003**, *100*, 8113.
- (55) Farrer, R. A.; Fourkas, J. T. *Acc. Chem. Res.* **2003**, *36*, 605.
- (56) Bellissent-Funel, M. C. *Eur. Phys. J. E* **2003**, *12*, 83.
- (57) Harpham, M. R.; Ladanyi, B. M.; Levinger, N. E.; Herwig, K. W. *J. Chem. Phys.* **2004**, *121*, 7855.
- (58) Dokter, A. M.; Woutersen, S.; Bakker, H. J. *Proc. Natl. Acad. Sci. U.S.A.* **2006**, *103*, 15355.
- (59) Park, S.; Moilanen, D. E.; Fayer, M. D. *J. Phys. Chem. B* **2008**, *112*, 5279.
- (60) Our simulation anisotropies are scaled to compensate for the different initial (<200 -fs) librational decays measured by the experiments and the simulations, which has no consequence for the remaining analysis.
- (61) The OD stretch vibrational lifetime was experimentally¹¹ confirmed to be unaffected by TMAO, which excludes a bias (shown for halides³⁵) of ultrafast anisotropy measurements toward a slower reorientation.
- (62) As explained at the end of section IV.b, at high concentration, the anisotropy decay is no longer strictly monoexponential because of the broad distribution of excluded volumes; here, we use the monoexponential approximation to compare the retardation factors from the simulations and the TSEV model.

JP809521T